Nanoscale

PAPER

View Article Online
View Journal | View Issue

Open Access Article. Published on 01 October 2025. Downloaded on 4/1/2026 3:22:40 PM.
This article is licensed under a Creative Commons Attribution 3.0 Unported Licence.

Check for updates

Cite this: *Nanoscale*, 2025, **17**, 24196

Tuning polysulfide adsorption and catalytic activity *via* surface functionalization of Nb_2TiN_2 MXene in Na–S batteries

Satheesh Mani and Md Mahbubul Islam *

Sodium–sulfur (Na–S) batteries are emerging as a promising candidate for large-scale energy storage due to the natural abundance and low cost of sodium and sulfur and their high theoretical energy density. However, the sluggish conversion kinetics of higher-order soluble polysulfides (Na_2S_n, $n > 2$) into lower-order insoluble species (Na_2S_2/Na_2S) lead to severe polysulfide dissolution, insulating discharge products, and rapid capacity fading. MXenes, a type of 2D transition metal carbides and nitrides, are a viable choice for cathode catalysts for Na–S batteries because of their high electrical conductivity and greater affinity towards polysulfides. Hence, in this study, we employ first-principles density functional theory (DFT) calculations to systematically investigate the adsorption characteristics and catalytic behavior of a novel double transition metal (DTM) nitride MXene, Nb_2TiN_2, functionalized with sulfur (S) and oxygen (O) terminal groups ($Nb_2TiN_2S_2$ and $Nb_2TiN_2O_2$, respectively). Our results reveal that O-functionalized $Nb_2TiN_2O_2$ exhibits significantly stronger adsorption of Na_2S_n species, which is expected to mitigate the shuttle effect and improve structural stability compared to its S-functionalized counterpart. Detailed analysis of adsorption energies and charge transfer mechanisms demonstrates that lower-order polysulfides exhibit stronger binding and higher electron transfer on the O-terminated surface. Furthermore, the calculated free energy barriers for the rate-determining step of S reduction reactions are significantly lower on the catalytic surfaces (0.55 eV for $Nb_2TiN_2O_2$ and 0.75 eV for $Nb_2TiN_2S_2$), than the barriers for the polysulfides conversion in the gas phase (1.05 eV). These findings suggest that O-functionalization facilitates more favorable reaction kinetics by stabilizing key intermediates and lowering energy barriers compared to S-functionalization. This work provides critical insights for the rational design of advanced cathode hosts to enhance the electrochemical performance and cycle life of Na–S batteries.

Received 17th July 2025,
Accepted 30th September 2025

DOI: 10.1039/d5nr03030g

rsc.li/nanoscale

1. Introduction

The growing demand for energy, as well as the environmental damage caused by fossil fuels, underscores the importance of finding sustainable alternatives. Renewable energy sources such as solar and wind provide clean energy; however, their intermittent nature necessitates the development of efficient and cost-effective energy storage systems. Developing such energy storage technology is critical to a sustainable future. Among the available options, rechargeable batteries stand out as the most viable solution to this challenge. Lithium-ion batteries are known for their high energy density. However, the energy density of traditional lithium-ion batteries using insertion-compound cathodes (*e.g.*, $LiCoO_2$, $LiMn_2O_4$, and $LiFePO_4$) and anode (graphite) is insufficient to meet the needs of electric vehicles and smart grids. As a result, novel battery chemistries are being aggressively investigated.[1]

Metal–sulfur (M–S) batteries are attracting increasing interest as next-generation energy storage systems due to their high theoretical specific discharge capacity (1672 mAh g^{-1}), energy density, low cost, and environmental sustainability.[2–4] Among these, lithium–sulfur (Li–S) chemistry has been extensively explored, with significant advancements achieved over the past decade. However, the high cost, limited availability, and geopolitical concerns surrounding lithium resources limit the scalability of Li–S batteries.[5–7] From both economic and sustainability perspectives, sodium (Na) presents a more promising alternative to lithium for pairing with sulfur cathodes, owing to its comparable chemical properties and substantially greater natural abundance.[8] Consequently, Na–S batteries hold strong potential for meeting the energy demands of a wide range of electrochemical applications, particularly large-scale grid energy storage.[9,10]

Department of Mechanical Engineering, Wayne State University, Detroit, Michigan 48202, USA. E-mail: gy5553@wayne.edu

This journal is © The Royal Society of Chemistry 2025

Open Access Article. Published on 01 October 2025. Downloaded on 4/1/2026 3:22:40 PM. This article is licensed under a Creative Commons Attribution 3.0 Unported Licence.

Despite advantages, the performance limiting factors of room temperature Na–S batteries – such as sluggish kinetics, poor rate capability, and rapid capacity degradation limit their practical realization.[10] These issues stem primarily from the shuttle effect and the poor conductivity of sulfur (5×10^{-28} S m^{-1}).[11] The former effect reduces the coulombic efficiency, leading to rapid capacity degradation due to the dissolution of soluble polysulfides during the charge and discharge cycles, and the latter slows down the kinetics of the reaction.[11] Furthermore, the significant volume expansion of sulfur (170%) disrupts the cathode structure, resulting in low cycle stability.[12] In order to overcome those limitations, it is necessary to develop anchoring materials (AMs) that can trap higher-order polysulfides within the cathode materials and catalyze the polysulfide conversion reactions. This would prevent their dissolution and improve the sluggish kinetics of the reversible conversion of short-chain polysulfides.[2,13] Various methods have been proposed to address these issues, such as the infusion of sulfur into the carbon matrices,[14] surface coating of sulfur through the introduction of additives into the cathode composition,[15] and optimization of the separators, interlayers, and electrolyte components. While these approaches can hinder polysulfide migration, they remain limited due to the weak chemical interaction between sulfur and nonpolar carbon.

In contrast, polar host materials, which exhibit intrinsic sulfidic properties, form strong chemical bonds with Na_2S_n, effectively preventing polysulfide shuttling. Two-dimensional (2D) materials such as graphene,[16] MoS_2,[17] WS_2,[18] phosphorene,[19] and others have been identified as potential AMs for Na–S batteries due to their high surface-to-volume ratio and tunable electrical properties.[20] Another class of 2D materials known as MXenes – with the general formula $M_{n+1}X_nT_x$ – has gained significant attention as potential AMs due to their high electronic conductivity, large surface area rich in active sites, tunable structural properties, and hydrophilicity. Here, M can be a transition metal such as Ti, Cr, V, Mo, or Nb; X can be carbon or nitrogen; and T stands for surface functional groups such as sulfur, oxygen, and fluorine.[21–24]

MXenes facilitate the efficient conversion of polysulfide intermediates, enhancing reaction kinetics and improving the electrochemical performance of sulfur-based batteries.[25,26] According to studies, MXenes can mitigate polysulfide dissolution in Na–S batteries by selectively interacting with sulfur species. Surface modification of MXenes can further enhance their ability to retain and trap polysulfides, effectively reducing the unwanted "shuttle effect".[24,27–29] For instance, Liang *et al.* investigated the electrochemical performance of $Ti_2C(OH)_x$/S sulfur electrodes.[30] Bao *et al.* suggested using 3D wrinkled S-doped MXene (S-$Ti_3C_2T_x$) nanosheets as a sulfur host.[31] Wang *et al.* systematically studied the electrochemical properties and lithium storage performance of various Ti_3C_2 MXenes where O- and S-functional groups co-exist.[32] DTM MXenes have recently garnered increased interest in the energy storage domain due to their unique structures, which feature two distinct transition metals at the M site. These materials are categorized into – ordered DTM MXenes (metals organized in particular layers, either in or out of plane) and solid solution DTM MXenes (metals scattered randomly).[33–35] Compared to conventional single-metal MXenes like $Ti_3C_2O_2$ or $Ti_3C_2S_2$, recently developed ordered DTM-MXenes offer a significantly broader compositional landscape, facilitating tailored electronic, magnetic, and catalytic properties.[36,37] The presence of two distinct transition metals introduces synergistic effects, including enhanced structural stability and tunable electronic properties. For instance, in contrast to $Ti_3C_2T_x$, the behavior of $Mo_2TiC_2T_x$ changes from metallic to semiconducting when Ti is substituted with Mo.[38] Also, it is reported that $Ti_3C_2T_x$ and other single transition metal MXenes exhibit limited capacity and cycling inefficiencies when used as Li-ion battery anode.[39,40] Zhou *et al.* found that ordered DTM-MXenes, such as MoWC and $MoWCO_2$, had considerably higher capacity and stability as an anode in Na-ion batteries. This improvement is due to the synergistic effect of dual-metal sites and the ordered crystal lattice resulting from unique atomic radii, which gives DTM-MXenes a significant advantage over their single-metal counterparts.[41] We previously investigated carbide-based MXenes, including $Ti_3C_2X_2$ (where X = S, O, F, and Cl)[42] and $Mo_2Ti_2C_2T_2$ (T = S and O)[21] for anchoring Li/Na polysulfides and polyselenides. Beyond carbide MXenes, nitride or carbonitride MXenes, especially those with DTM, offer superior electrochemical performance due to their higher conductivity, faster ion transport, and improved surface wettability, leading to more active sites for reactions.[43] However, the research on DTM-nitride and carbonitride MXene is still limited. In our previous research, we reported the discovery of a novel DTM-nitride based MXene functionalized with S group ($Nb_2TiN_2S_2$), which demonstrated an excellent anchoring ability for Li_2Se_n species in Li–Se batteries.[44] Building on this, herein, we investigated the binding mechanism and reaction kinetics of Na_2S_n species on both S- and O-functionalized Nb_2TiN_2 MXenes for Na–S batteries.

In this study, we employ first-principles density functional theory (DFT) to investigate the potential of DTM-nitride MXenes —specifically S and O functionalized $Nb_2TiN_2S_2$ and $Nb_2TiN_2O_2$—as AMs for trapping and catalyzing polysulfides in Na–S batteries. We begin by calculating the adsorption energies of various intermediate polysulfides, followed by an analysis of the charge transfer mechanisms through Bader charge calculations. Additionally, we explore the conductive nature of the AM after Na_2S_n adsorption by evaluating the density of states (DOS). To further understand the sulfur reduction reaction (SRR) during the discharge process, we compute and analyze the Gibbs free energy profiles. This study provides a comprehensive theoretical foundation for future experimental research on DTM-nitride MXenes in energy storage applications.

2. Calculation methodology

The Vienna *Ab initio* Simulation Package (VASP) was utilized to perform spin-polarized DFT calculations. The Perdew–Burke–

Open Access Article. Published on 01 October 2025. Downloaded on 4/1/2026 3:22:40 PM. This article is licensed under a Creative Commons Attribution 3.0 Unported Licence.

Ernzerhof (PBE) functional was employed to evaluate the exchange–correlation energy within the generalized gradient approximation (GGA) framework. The Projector Augmented Wave (PAW) method was applied to account for the influence of core electrons on the valence electron density. A plane-wave kinetic energy cutoff of 520 eV was used for the calculations. To incorporate van der Waals (vdW) interactions, the DFT-D3 method with zero damping (IVDW = 11) and empirical dispersion correction was implemented. A vacuum layer of 25 Å was introduced in the out-of-plane direction to eliminate interactions between periodic images. Geometry optimizations were performed using the conjugate gradient method, allowing for atomic relaxation until the forces acting on all atoms were minimized to below 0.025 eV Å^{-1}, with energy convergence achieved below 1×10^{-4} eV. The Monkhorst–Pack grid scheme was employed to sample the Brillouin zone for both electronic structure calculations and atomic relaxations. We employed a $3 \times 3 \times 1$ k-point mesh for all the adsorption energy calculations and $11 \times 11 \times 1$ k-point mesh for all electronic state calculations. Bader charge analysis was conducted to examine charge transfer between Na_2S_n and the AMs, with the difference in charge density calculated using the specified equation.

$$\rho_b = \rho_{\text{adsorbed state}} - (\rho_{\text{absorbate}} + \rho_{AM})$$

where $\rho_{\text{adsorbed state}}$, $\rho_{\text{absorbate}}$, and ρ_{AM} represent the charge density of the Na_2S_n adsorbed AM, the isolated polysulfides, and the adsorption material, respectively. The Gibbs free energy (ΔG) for SRR during the Na–S discharge process is calculated as $\Delta G = \Delta E + \Delta ZPE - T\Delta S$, where ΔE represents the adsorption energy and ΔZPE and $T\Delta S$ denote the zero-point energy difference and entropy difference between the gas phase and adsorbed phase, calculated by using VASPKIT[45] at 298.15 K. The detail procedure for calculating the SRR free energies are described in our previous publications.[2] The atomic visualization and charge density differences were carried out with the VESTA code.[46]

3. Results and discussion

3.1. Polysulfide adsorption on $Nb_2TiN_2T_2$ (T = S and O)

During the discharge phase of the Na–S battery, Na reacts with the elemental S_8, leading to the formation of a series of intermediates, specifically Na_2S_n (where n = 1, 2, 4, 6, 8). To investigate the anchoring characteristics of $Nb_2TiN_2T_2$ (T = S and O), the adsorption energies of both S_8 and the Na_2S_n species were computed using $E_{ads} = E_{Na_2S_n} + E_{AM} - E_{Na_2S_n+AM}$, where $E_{Na_2S_n}$, E_{AM}, and $E_{Na_2S_n+AM}$ denote the DFT energies of isolated Na_2S_n, AM, and the polysulfide adsorbed AM, respectively. The Nb_2TiN_2 monolayer has a quint-layer structure, with two nitrogen (N) layers encasing a Ti atomic layer. Niobium (Nb) layers enclose the N layers on the top and bottom surfaces in the order Nb–N–Ti–N–Nb. The Nb_2TiN_2 monolayer underwent structural relaxation, and the optimal lattice constants were found to be $a = b$ = 3.01 Å, with a layer thickness of 5.08 Å (ref. 44) (see Fig. S1). Bare MXenes are reported to exhibit significantly high adsorption energies, which can lead to the decomposition of polysulfides.[31,42] To address this, S and O functional groups are introduced on the surfaces of the Nb layer, and their effects on electrochemical performance were investigated. In our previous research on Nb_2TiN_2-MXene with S group, we determined that the adsorption site directly above the N atom was thermodynamically stable. This conclusion was based on calculated formation energy values for N-top site (approximately −6.0 eV), when compared to the other two sites (*i.e.*, specifically above Ti and Nb). Based on this finding, we considered S and O above the N atom sites for $Nb_2TiN_2S_2/O_2$.[44]

In Nb_2TiN_2 structure, the Nb and Ti atoms are arranged in separate layers, with Nb metal occupying the outer layers and the other Ti metal being filled in the inner layers. Fig. 1 show the relaxed configurations for S_8 and Na_2S_n adsorbed $Nb_2TiN_2S_2/O_2$. It is clear that during adsorption, the structures of Na_2S_n species are preserved. With a minimum spacing of approximately 3 to 3.5 Å, the S_8 adsorbed parallel to the AMs. The distance between the S_8 molecule and the $Nb_2TiN_2S_2$ and $Nb_2TiN_2O_2$ surfaces is 3.52 and 3.08 Å, respectively, which is greater than the combined atomic radii of S atoms (1.00 Å). This indicates a weak binding dominated by vdW forces. In contrast, other Na_2S_n molecules adsorb on $Nb_2TiN_2T_2$ (T = S and O) with their Na atoms oriented toward the S atoms on the surface. The Na–S distances are shown in Table 1. The Na_2S_n is found to be adsorbed at the bridging site, where each Na atom forms a strong Na–O (in $Nb_2TiN_2O_2$) and Na–S (in $Nb_2TiN_2S_2$) bonds with the substrate. Notably, the atomic radii of Na and S atoms are 1.80 Å and 1.00 Å, respectively. Therefore, the Na_2S_n–$Nb_2TiN_2S_2/O_2$ distances are close to the sum of these radii, indicating stronger chemical interactions.[47] The statement is further supported by the calculated adsorption energies (E_{ads}) of S_8 and Na_2S_n adsorbed on S and O functionalized MXene ($Nb_2TiN_2S_2/O_2$), as depicted in Fig. 2. As the sodiation process proceeds, the adsorption energies on both substrates show a gradual rise. In particular, the adsorption strength increases approximately linearly from higher-order (n = 8) to lower-order (n = 1) polysulfides except for Na_2S_6. A consistent trend we observed in metal–S batteries is that lower-order polysulfides like Na_2S and Na_2S_2 exhibit stronger adsorption on MXene surfaces compared to higher-order polysulfides. The shorter chain lengths result in enhanced electrostatic interactions with the negatively charged surface atoms of MXenes.[42,48]

To gain deeper insights into the effect of surface terminations, we compared the adsorption energies of Na_2S_n on S and O-functionalized MXenes. These results indicate that lower-order polysulfides, such as Na_2S and Na_2S_2, exhibit stronger adsorption on the O-terminated surface than on the S-terminated counterpart. Notably, the adsorption energies of Na_2S_2 and Na_2S on $Nb_2TiN_2O_2$ were found to be 4.33 and 4.23 eV, compared to 3.00 and 3.56 eV on $Nb_2TiN_2S_2$, respectively. Overall, the O-functionalized MXene shows higher binding affinity towards Na_2S_n than the S-functionalized one. The significantly higher adsorption energy observed for $Nb_2TiN_2O_2$ MXenes primarily stems from the higher electronegativity of O

Open Access Article. Published on 01 October 2025. Downloaded on 4/1/2026 3:22:40 PM.
This article is licensed under a Creative Commons Attribution 3.0 Unported Licence.

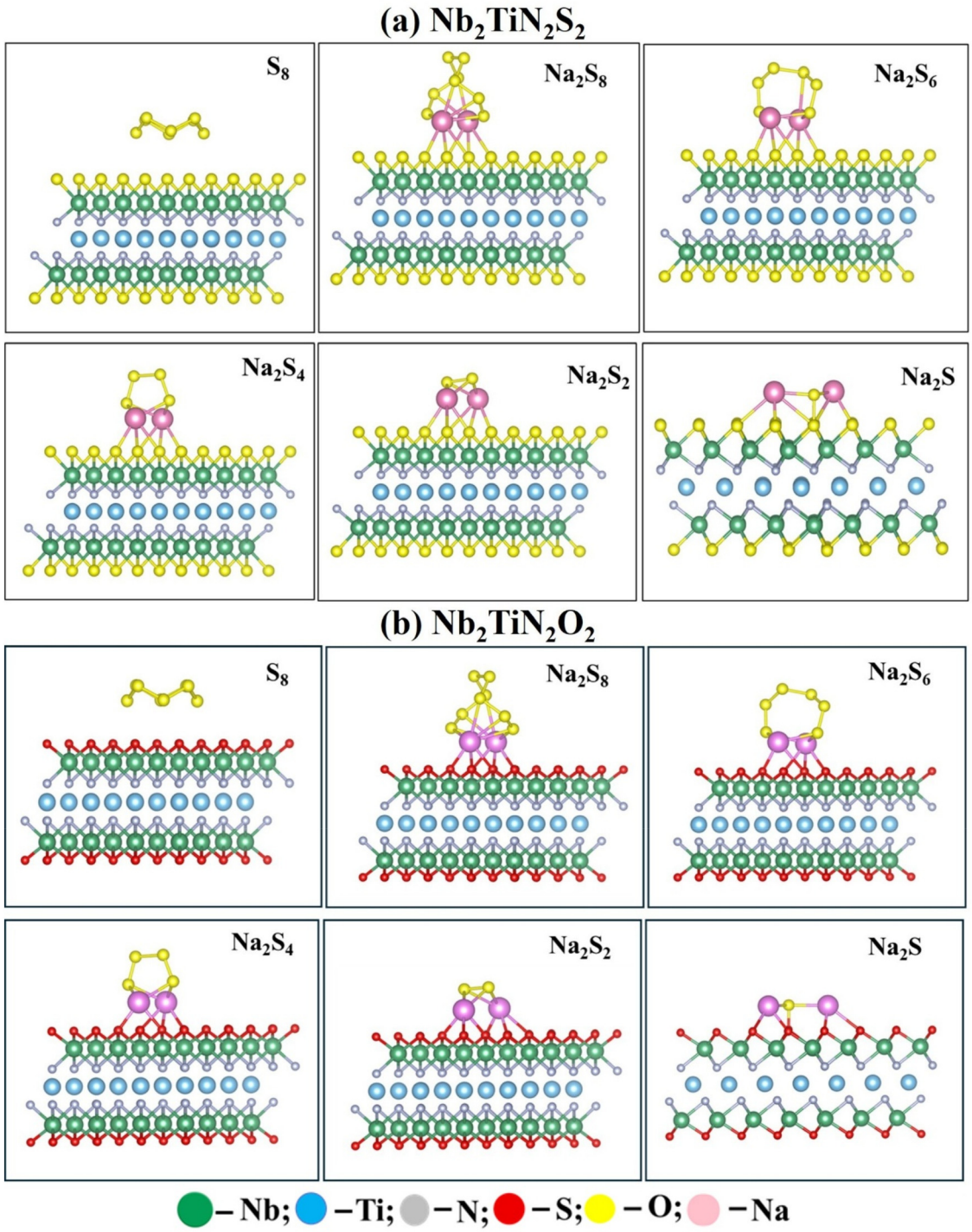

Fig. 1 Optimized geometric configurations of S_8 and Na_2S_n adsorbed on (a) $Nb_2TiN_2S_2$; (b) $Nb_2TiN_2O_2$.

compared to S. On the Pauling scale, O and S have electronegativities of 3.44 and 2.58, respectively.[49] This higher electronegativity means that O atoms more effectively attract electron density from the underlying transition metal MXene framework (such as Ni and Ti), leading to a more negatively charged surface. This increased negative charge enhances electrostatic interactions with the positively charged sodium present in Na_2S_n species, leading to stronger adsorption. As a result, these interactions reduce the dissolution of polysulfides and provide a mechanism for suppressing the shuttle effect.

To evaluate the effectiveness of $Nb_2TiN_2T_2$ (T = S and O) in mitigating the shuttle effect, the adsorption energies of Na_2S_n with common electrolyte solvents such as 1,3-dioxolane (DOL) and 1,2-dimethoxymethane (DME) were calculated and com-

Open Access Article. Published on 01 October 2025. Downloaded on 4/1/2026 3:22:40 PM.
This article is licensed under a Creative Commons Attribution 3.0 Unported Licence.

Table 1 Calculated variation in the average Na–S bond distance (Δd_{Na-S}) in Na_2S_n and the minimum distance between the S_8/Na_2S_n species ($d_{Na_2S_n-AM}$) (in Å) and the $Nb_2TiN_2S_2/O_2$ substrates

	Δd_{Na-S}		$d_{Na_2S_n-AM}$	
Na_2S_n	$Nb_2TiN_2S_2$	$Nb_2TiN_2O_2$	$Nb_2TiN_2S_2$	$Nb_2TiN_2O_2$
S_8	—	—	3.52	3.08
Na_2S_8	3.01	3.07	2.86	2.36
Na_2S_6	2.95	2.88	2.94	2.35
Na_2S_4	2.84	2.93	2.78	2.33
Na_2S_2	2.80	3.17	2.80	2.32
Na_2S	2.78	2.80	2.70	2.34

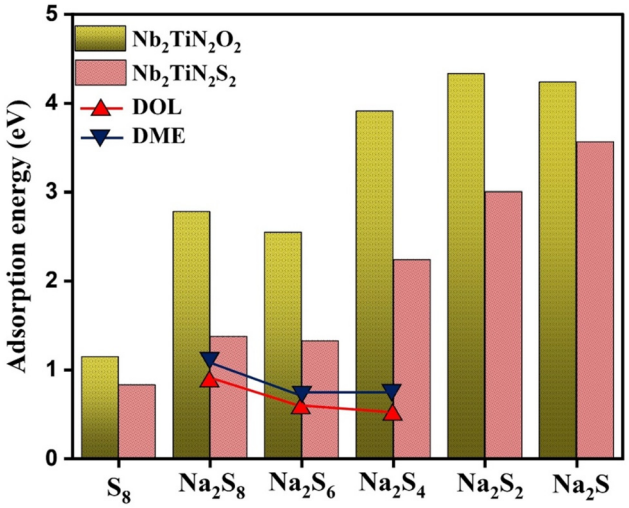

Fig. 2 The calculated adsorption energies of S_8 and Na_2S_n adsorbed on $Nb_2TiN_2T_2$. The binding energies of higher-order Na_2S_n with the electrolyte solvents DOL and DME are taken from ref. 2

pared. The comparatively higher binding energy values with the AMs, as opposed to those of Na_2S_n with DME and DOL, effectively ensure the inhibition of the shuttle effect. The configurations of DOL and DME adsorbed structures, which involve higher-order M_2X_n interactions through a single bond, were previously reported in our previous works.[50,51] Since $Nb_2TiN_2T_2$ contains transition-metal d orbitals, typically GGA with a Hubbard U correction is necessary to properly account for on-site Coulomb interactions. However, our previous studies on $Mo_2TiC_2T_2$ (T = O, S), $Ti_3C_2T_2$ (T = O, S, F, Cl), VS_2, and MoS_2 have demonstrated that inclusion of U parameters has a negligible effect on the binding energies of polychalcogenides.[2,21,42,51] To further assess this effect, we calculated the polysulfides binding energies on $Nb_2TiN_2T_2$ (T = O, S) using U = 4.0 eV for Ti and 2.0 eV for Nb, consistent with prior studies.[52–54] As shown in Fig. S2, the results demonstrate that incorporating U parameters has an insignificant influence on polysulfide interactions. Therefore, we conclude that the PBE functional without U corrections is adequate to describe Na_2S_n adsorption on $Nb_2TiN_2T_2$ surfaces. To further examine solvation effects, we performed simulations using the continuum solvation model in VASPsol considering the dielectric constant of DME (ε = 7.2). The results are presented in Fig. S3 reveal that implicit solvation has a negligible effect on the predicted polysulfide binding energies on $Nb_2TiN_2T_2$ (T = O, S). Therefore, we find that gas-phase calculations are sufficient to describe polysulfide interactions.

Although the predicted adsorption energies of sodium polysulfides on DTM-MXenes are relatively high—raising potential concerns about strong adsorption and hindered SRR kinetics—literature evidence indicates that these values remain within the desirable range. According to the Sabatier principle, adsorption should be neither too weak (leading to polysulfide shuttling) nor too strong (causing site poisoning). In our study, the reported binding energies fall within this optimal window. For example, Nahian *et al.* reported comparable binding energies (~4.0–4.5 eV) for lower-order polysulfides (Na_2S_2 and Na_2S) on $Mo_2TiC_2O_2$ surfaces, which yet correlated with enhanced SRR activity.[21] Similarly, Deng *et al.* found binding energy values in the range of 3–7 eV for metal-MOF centres.[55] Recently, Song *et al.* reported Na_2S_4 binding energies up to 7.53 eV for Fe–N_x catalysts for Na–S batteries with enhanced sulfur utilization (81.4% at 167.5 mA g^{-1}), superior rate performance (1003.0 mAh g^{-1} at 1675 mA g^{-1}), and stable long-term cycling (83.5% retention over 450 cycles).[56] Additionally, our computed reaction free-energy profile clearly demonstrates that SRR occurs more effectively on DTM MXenes than under vacuum conditions. Together, these results confirm that the adsorption energies reported here are not expected to retard SRR.

3.2. Charge transfer analysis for the polysulfides adsorption on $Nb_2TiN_2O_2$ and $Nb_2TiN_2S_2$

To examine the charge transfer process during the adsorption of S_8 and Na_2S_n species on $Nb_2TiN_2S_2/O_2$ substrates, Bader charge analysis was conducted, and the results are shown in Fig. 3. This electron transfer is critical for understanding binding strength and covalent interactions between Na_2S_n and the AM. The positive charge transfer values indicate electron transfer from S_8 and Na_2S_n species to the AMs. Our results showed a clear pattern of increased charge transfer from S_8 to lower-order polysulfides (Na_2S), indicating stronger interactions as the polysulfide chain shortens. An exception to this trend occurs with Na_2S_6 on $Nb_2TiN_2O_2$, where the charge transfer (~1.1e) is slightly lower than that of Na_2S_8 (~1.29e). The charge transfer from S_8 to $Nb_2TiN_2S_2$ (0.145e) and $Nb_2TiN_2O_2$ (0.26e) is relatively low in both cases, indicating a weak electrostatic interaction between the S_8 molecule and the substrate. The minimal charge redistribution indicates that physisorption takes precedence over strong chemisorptive binding, indicating a limited adsorption strength of S_8 on both surfaces. However, the O-functionalized $Nb_2TiN_2O_2$ surface has slightly greater charge transfer, indicating stronger adsorption compared to the S-functionalized counterpart. This is likely owing to enhanced electronic affinity introduced by the O-terminal groups.

 This journal is © The Royal Society of Chemistry 2025

Open Access Article. Published on 01 October 2025. Downloaded on 4/1/2026 3:22:40 PM.
This article is licensed under a Creative Commons Attribution 3.0 Unported Licence.

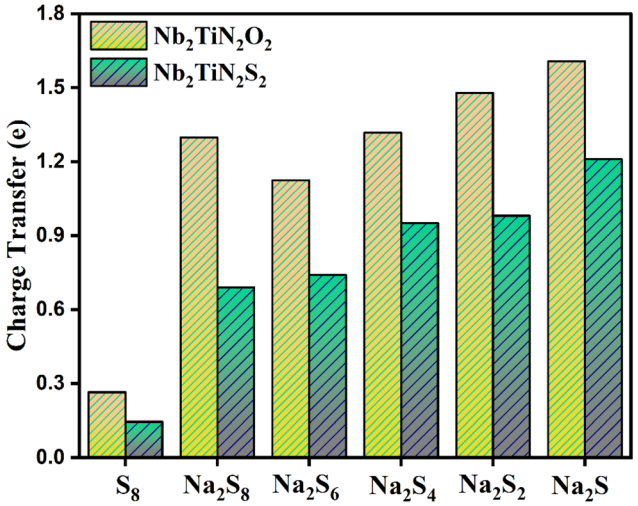

Fig. 3 Computed charge transfer for S_8 and Na_2S_n adsorbed $Nb_2TiN_2S_2/O_2$.

Across all sulfur species investigated, $Nb_2TiN_2O_2$ consistently exhibits a higher degree of charge transfer compared to $Nb_2TiN_2S_2$. Specifically, for higher-order polysulfides such as Na_2S_8 and Na_2S_6, the charge transfer on $Nb_2TiN_2O_2$ is approximately $1.29|e|$ and $1.13|e|$, respectively, which is markedly higher than the corresponding values of $\sim 0.69|e|$ and $\sim 0.74|e|$ observed for $Nb_2TiN_2S_2$. This trend continues through the intermediate species Na_2S_4 and Na_2S_2, where $Nb_2TiN_2O_2$ exhibits charge transfer values of $1.30|e|$ and $1.50|e|$, respectively, in contrast to $0.95|e|$ and $0.98|e|$ observed for $Nb_2TiN_2S_2$. The disparity becomes most pronounced with Na_2S, for which $Nb_2TiN_2O_2$ reaches a peak charge transfer of $\sim 1.60|e|$, significantly surpassing the $\sim 1.20|e|$ observed on $Nb_2TiN_2S_2$. Higher charge transfer indicates a stronger electronic coupling between $Nb_2TiN_2O_2$ and Na-polysulfides, which leads to improved adsorption and catalysis during electrochemical processes.

This conclusion is reinforced by the differential charge density analysis as shown in Fig. 4. The figure illustrates various Na_2S_n (Na_2S_8, Na_2S_6, Na_2S_4, Na_2S_2, Na_2S) adsorbed on the $Nb_2TiN_2S_2/O_2$ catalyst, with yellow regions indicating charge accumulation and cyan regions showing depletion. Our findings reveal that charge transfer from the Na_2S_n species to the catalyst was primarily driven by S atoms rather than metal ions in both the O and S functionalized substrates, which emphasizes the specific mechanism behind this interaction. This aligns with our previous research on Na–S battery systems employing $Mo_2TiC_2S_2$ MXene as an AM.[2] Furthermore, the extent of charge transfer is found to be more pronounced on the O-functionalized substrate than on the S-functionalized one, which corroborates the stronger electronic interactions and affinity of S atoms in polysulfides towards the more electronegative O-functionalized AM. Overall, $Nb_2TiN_2O_2$ demonstrates a stronger binding than $Nb_2TiN_2S_2$ as revealed through the charge transfer analysis.

3.3. Sulfur reduction reaction (SRR)

During the discharge process of Na–S batteries, we investigated the complete reaction pathway, including the formation of

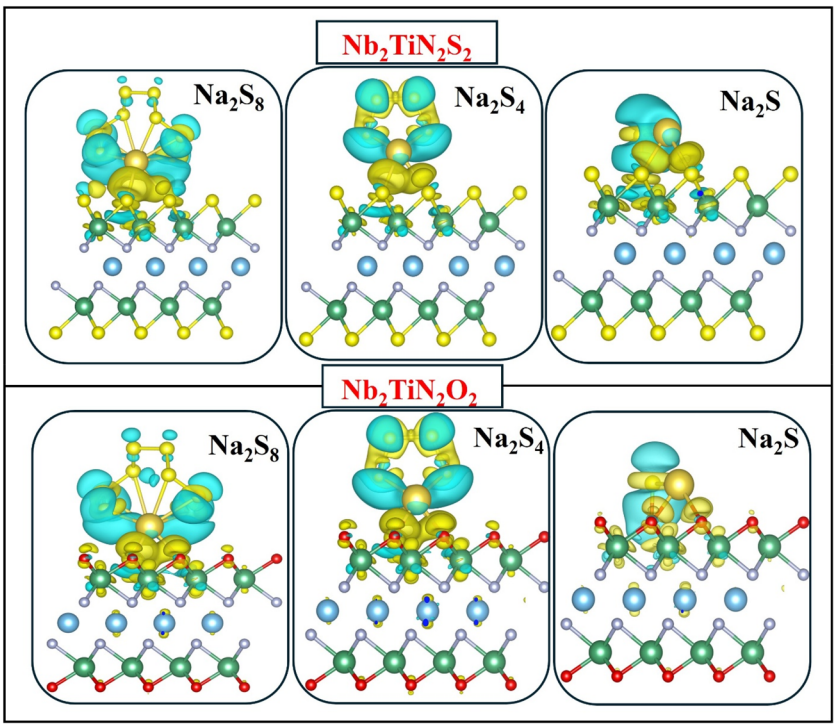

Fig. 4 Charge density differences of Na_2S_8, Na_2S_4 and Na_2S on $Nb_2TiN_2S_2/O_2$. The isosurface level is set at 0.001 e Å^{-3}.

Open Access Article. Published on 01 October 2025. Downloaded on 4/1/2026 3:22:40 PM.
This article is licensed under a Creative Commons Attribution 3.0 Unported Licence.

Na_2S_n from S_8 and bulk Na, to gain insight into the SRR kinetics on $Nb_2TiN_2S_2$ and $Nb_2TiN_2O_2$ surfaces. We computed the free energy change (ΔG) for each intermediate reaction step, both in the gas phase and on $Nb_2TiN_2S_2/O_2$ substrates. By determining the extent to which the $Nb_2TiN_2S_2/O_2$ surface reduces energy barriers and stabilizes important intermediates in comparison to the gas phase baseline, this comparative analysis enabled us to evaluate the catalytic efficacy of the substrates. In Na–S batteries, the conversion of high-order soluble polysulfides to low-order insoluble polysulfides is often limited by sluggish reaction kinetics, which contributes to the polysulfide shuttling effect.[57] Fig. 5 illustrates the ΔG profile along the reaction pathway from S_8 to Na_2S. It is evident from the figure that the initial step, involving the reduction of S_8 to Na_2S_8, is spontaneously exothermic in all three cases, with the ΔG values calculated as −4.28 eV in the gas phase, −4.93 eV on $Nb_2TiN_2S_2$, and −5.05 eV on $Nb_2TiN_2O_2$. Similarly, the conversion of Na_2S_8 to Na_2S_6 is also exothermic, with ΔG values of −0.05 eV and −0.01 eV on S and O-functionalized surfaces, respectively. In contrast, the same step is uphill in the gas phase with a positive ΔG of 0.14 eV. Furthermore, the Na_2S_6 to Na_2S_4 conversion shows an increasing trend in free energy in the gas phase (ΔG rising from 0.14 to 0.82 eV), whereas it proceeds spontaneously with negative ΔG values on both $Nb_2TiN_2S_2$ (−0.19 eV) and $Nb_2TiN_2O_2$ (−0.57 eV) AMs. Between the two AMs, the O-functionalized surface demonstrates faster reaction kinetics, as evident from the lower energy barriers.

Since Na_2S_4 is a soluble liquid-phase species and Na_2S_2 precipitates as an insoluble solid product,[58] the conversion of Na_2S_4 to Na_2S_2 emerges as the rate-determining step. This step exhibits ΔG values of 0.75 eV and 0.55 eV on S and O-functionalized surfaces, respectively, indicating a transition from exothermic polysulfide conversion reactions to endothermic behavior depending on the surface chemistry. Though both functionalized materials effectively promote the early stages of polysulfide conversion, a kinetic bottleneck arises at this critical step, which limits the overall reaction rate and battery performance. However, compared to the gas phase, the $Nb_2TiN_2S_2$ surface reduces the energy barrier for the Na_2S_4 to Na_2S_2 conversion by 48%, and $Nb_2TiN_2O_2$ achieves an even greater reduction of 66%, highlighting their significant role in enhancing the electrochemical performance of the Na–S system. The final conversion step from Na_2S_2 to Na_2S exhibits an uphill trend in the free energy profile, indicating an endothermic process across all three phases. The positive ΔG associated with this step suggests that it is non-spontaneous and requires an external thermodynamic driving force to proceed. This behavior may arise from the relative stabilization of Na_2S_2 intermediates or the comparatively weaker interaction of Na_2S with the AM. Overall, the SRR is more thermodynamically favorable in the presence of AMs than under gas-phase conditions. Among the two functionalized surfaces, the O-terminated Nb_2TiN_2 consistently outperforms the S-functionalized counterpart by more effectively lowering the activation barriers at each intermediate stage, thereby promoting faster SRR kinetics during the Na–S battery discharge. We calculated the Gibbs free energies for all reaction steps on $Nb_2TiN_2S_2/O_2$ substrates and then compared them to gas phase data (Fig. 5). A detailed description of the Gibbs free energy calculation methodology can be found in our previous study.[2]

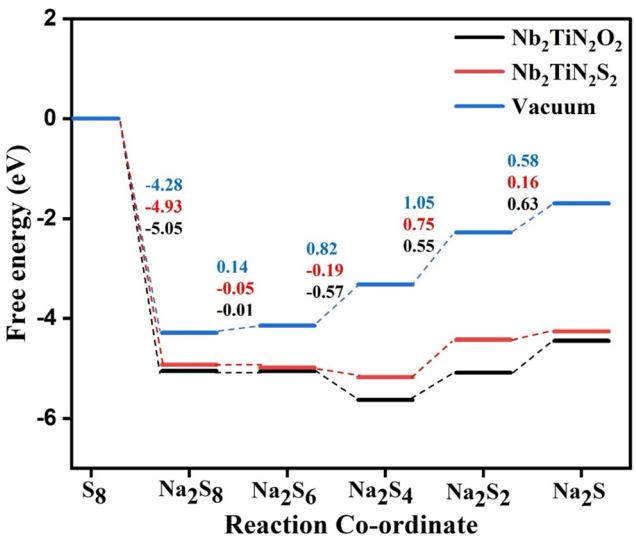

Fig. 5 Gibbs free energy profile of sulfur reduction reaction in vacuum and on $Nb_2TiN_2S_2/O_2$.

3.4. Electronic structure analysis

For the Na–S system on a $Nb_2TiN_2S_2/O_2$ substrate, partial density of states (PDOS) analysis provides important information on the electronic structure and interactions in the system. Fig. 6 and 7 show a detailed understanding of PDOS for S_8 and Na_2S_n on a $Nb_2TiN_2S_2$ and $Nb_2TiN_2O_2$ substrate, respectively. For S-functionalized MXene, significant electronic states are present in the system at the Fermi level, suggesting that metallic behavior and strong electronic conductivity are two essential components needed for improving charge transfer in Na–S batteries. The extent of orbital overlap between the Na–S system and AM was assessed by examining PDOS contributions from S(3p), Ti(3d), Nb(4d), and N(2p) atoms. PDOS analysis was performed for each polysulfide (both soluble and insoluble) and observed that key contributions near the Fermi level arise primarily from the Ti-3d orbitals, suggesting Ti's dominant role in determining the electronic properties of the system. In addition, Nb-4d orbitals also contribute near the Fermi level, indicating the importance of this Nb atom in shaping the overall electronic structure and establishing covalent interactions with S atoms. When Na_2S_n is adsorbed, peaks appear below the Fermi level, indicating charge transfer from Na_2S_n to $Nb_2TiN_2S_2$. This transfer is primarily attributed to the hybridization between the p orbitals of Na and S.

For the O-functionalized counterpart, $Nb_2TiN_2O_2$, a similar metallic character is retained post Na_2S_n adsorption. However, in this case, the PDOS reveals a dominant contribution from the Nb-4d orbitals, accompanied by nearly equivalent contri-

 This journal is © The Royal Society of Chemistry 2025

Open Access Article. Published on 01 October 2025. Downloaded on 4/1/2026 3:22:40 PM.
This article is licensed under a Creative Commons Attribution 3.0 Unported Licence.

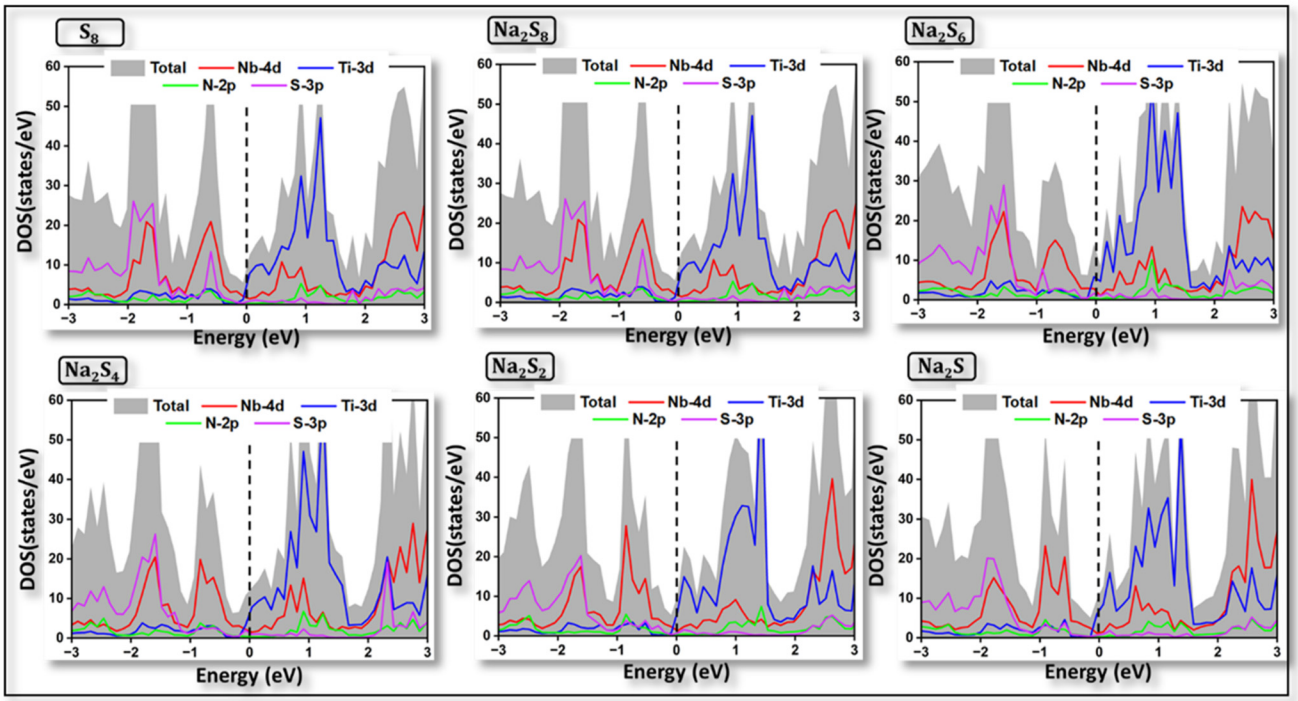

Fig. 6 PDOS of S_8 and Na_2S_n adsorbed on $Nb_2TiN_2S_2$. The Fermi level is denoted by vertical lines.

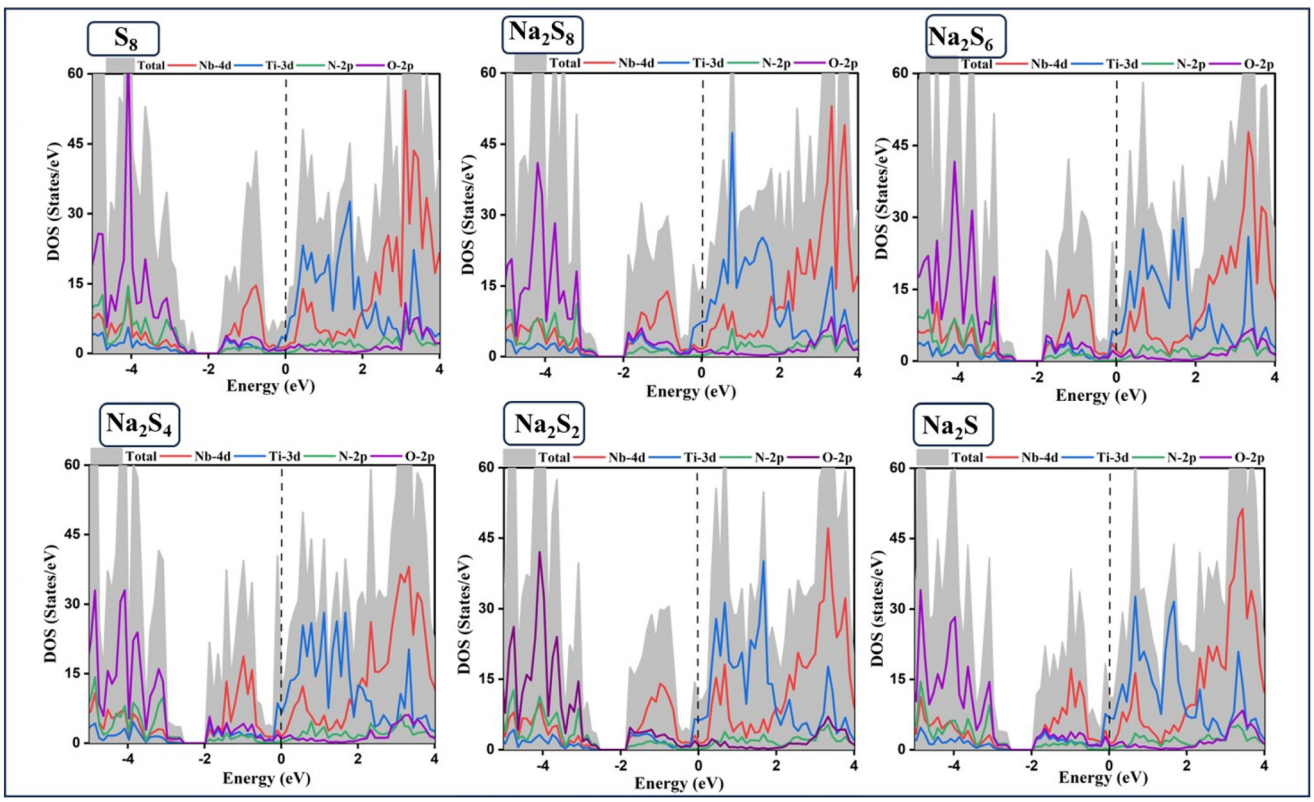

Fig. 7 PDOS of S_8 and Na_2S_n (n = 1, 2, 4, 6, and 8) adsorbed on $Nb_2TiN_2O_2$. The Fermi level is denoted by vertical lines.

Open Access Article. Published on 01 October 2025. Downloaded on 4/1/2026 3:22:40 PM.
This article is licensed under a Creative Commons Attribution 3.0 Unported Licence.

butions from Ti-3d orbitals. This indicates that in the O-functionalized system, both Nb and Ti play synergistic roles in defining the electronic properties and enhancing interfacial bonding. The PDOS analysis indicates that the Na–S system retains its metallic character upon adsorption on both $Nb_2TiN_2S_2$ and $Nb_2TiN_2O_2$ substrates, predominantly due to Ti-3d states in the S-functionalized case, and due to combined contributions from Nb-4d and Ti-3d states in the O-functionalized case.

4. Conclusion

The widespread utilization of the Na–S system is restricted by the shuttle effect and sluggish reaction kinetics. To address this issue, we employed DFT calculations to investigate the adsorption energy and reaction kinetics of Na_2S_n species on our computationally discovered S and O-functionalized $Nb_2TiN_2T_2$ (T = S, O) substrates.[44] Adsorption energy calculation revealed that both the surface group exhibits strong interaction with Na_2S_n; however, $Nb_2TiN_2O_2$ exhibits superior binding energies compared to $Nb_2TiN_2S_2$, Thus, $Nb_2TiN_2O_2$ is expected to effectively mitigate the shuttle effect. Furthermore, upon Na_2S_n adsorption, both substrates maintain their structural rigidities without any structural deformation, which is crucial for ensuring high reversibility during the redox reactions. Bader and charge density difference analysis further revealed a significant amount of electrons transferred from Na_2S_n to both the substrates, especially for lower order insoluble polysulfides, with the O-surface exhibiting a strong covalent interaction due to higher charge redistribution. Gibbs free energy, ΔG, profiles for the SRR revealed that the rate-determining step ($Na_2S_4 \rightarrow Na_2S_2$) is more favorable on both $Nb_2TiN_2S_2$ and $Nb_2TiN_2O_2$ substrates compared to the gas phase, with the O-functionalized surface exhibiting superior catalytic performance by achieving 66% reduction barrier improvement *versus* 48% for the S-functionalized counterpart. Besides, PDOS study revealed that $Nb_2TiN_2S_2/O_2$ AM retains their metallic nature post Na_2S_n adsorption. Which is essential for effective charge transfer during battery operation. In conclusion, both $Nb_2TiN_2S_2$ and $Nb_2TiN_2O_2$ substrates demonstrate strong potential as AM for Na–S batteries *via* offering enhanced binding strength, increased charge transfer, and faster kinetics. Among them, the O-functionalized $Nb_2TiN_2O_2$ outperforms the S-functionalized, highlighting the importance of surface termination in tuning MXene-based materials for high-performance and stable metal–S batteries.

Conflicts of interest

There are no conflicts of interest to declare.

Data availability

The authors confirm that the data required to reproduce the findings of this study are available within the article and can be reproduced by density functional theory calculations.

Supplementary information includes the optimized geometric configurations of pristine and surface-functionalized DTM-MXenes, comparison of adsorption energies of S_8 and Na_2S_n (n = 2, 4, 6, and 8) for O- and S-functionalized groups employing Hubbard corrections (PBE and PBE+U), and comparison of polysulfide adsorption energies between the gas phase and the implicit solvation model. See DOI: **https://doi.org/10.1039/d5nr03030g**.

Acknowledgements

This work is partially supported by the National Science Foundation (Award No. CBET-2400109).

References

1 A. Manthiram, S.-H. Chung and C. Zu, Lithium–Sulfur Batteries: Progress and Prospects, *Adv. Mater.*, 2015, **27**(12), 1980–2006, DOI: **10.1002/adma.201405115**.
2 R. Jayan and M. M. Islam, Mechanistic Insights into Interactions of Polysulfides at VS2 Interfaces in Na–S Batteries: A DFT Study, *ACS Appl. Mater. Interfaces*, 2021, **13**(30), 35848–35855, DOI: **10.1021/acsami.1c10868**.
3 A. Manthiram, Y. Fu, S.-H. Chung, C. Zu and Y.-S. Su, Rechargeable Lithium–Sulfur Batteries, *Chem. Rev.*, 2014, **114**(23), 11751–11787, DOI: **10.1021/cr500062v**.
4 M. S. Syali, D. Kumar, K. Mishra and D. K. Kanchan, Recent Advances in Electrolytes for Room-Temperature Sodium-Sulfur Batteries: A Review, *Energy Storage Mater.*, 2020, **31**, 352–372, DOI: **10.1016/j.ensm.2020.06.023**.
5 S. Wenzel, H. Metelmann, C. Raiß, A. K. Dürr, J. Janek and P. Adelhelm, Thermodynamics and Cell Chemistry of Room Temperature Sodium/Sulfur Cells with Liquid and Liquid/Solid Electrolyte, *J. Power Sources*, 2013, **243**, 758–765, DOI: **10.1016/j.jpowsour.2013.05.194**.
6 I. Kim, J.-Y. Park, C. H. Kim, J.-W. Park, J.-P. Ahn, J.-H. Ahn, K.-W. Kim and H.-J. Ahn, A Room Temperature Na/S Battery Using a B″ Alumina Solid Electrolyte Separator, Tetraethylene Glycol Dimethyl Ether Electrolyte, and a S/C Composite Cathode, *J. Power Sources*, 2016, **301**, 332–337, DOI: **10.1016/j.jpowsour.2015.09.120**.
7 S. Wei, S. Xu, A. Agrawral, S. Choudhury, Y. Lu, Z. Tu, L. Ma and L. A. Archer, A Stable Room-Temperature Sodium–Sulfur Battery, *Nat. Commun.*, 2016, **7**(1), 11722, DOI: **10.1038/ncomms11722**.
8 L. Li, K. H. Seng, D. Li, Y. Xia, H. K. Liu and Z. Guo, SnSb@carbon Nanocable Anchored on Graphene Sheets for Sodium Ion Batteries, *Nano Res.*, 2014, **7**(10), 1466–1476, DOI: **10.1007/s12274-014-0506-z**.

 This journal is © The Royal Society of Chemistry 2025

Open Access Article. Published on 01 October 2025. Downloaded on 4/1/2026 3:22:40 PM.
This article is licensed under a Creative Commons Attribution 3.0 Unported Licence.

9 D. Kumar, S. B. Kuhar and D. K. Kanchan, Room Temperature Sodium-Sulfur Batteries as Emerging Energy Source, *J. Energy Storage*, 2018, **18**, 133–148, DOI: 10.1016/j.est.2018.04.021.

10 Y. X. Wang, J. Yang, W. Lai, S. L. Chou, Q. F. Gu, H. K. Liu, D. Zhao and S. X. Dou, Achieving high-performance room-temperature sodium–sulfur batteries with S@ interconnected mesoporous carbon hollow nanospheres, *J. Am. Chem. Soc.*, 2016, **138**(51), 16576–16579, DOI: 10.1021/jacs.6b08685.

11 S. Ren, P. Sang, W. Guo and Y. Fu, Organosulfur Polymer-Based Cathode Materials for Rechargeable Batteries, *Polym. Chem.*, 2022, **13**(40), 5676–5690, DOI: 10.1039/D2PY00823H.

12 K. Tang, X. Peng, S. Chen, F. Song, Z. Liu, J. Hu, X. Xie and Z. Wu, Hierarchically Porous Carbon Derived from Delignified Biomass for High Sulfur-Loading Room-Temperature Sodium-Sulfur Batteries, *Renewable Energy*, 2022, **201**, 832–840, DOI: 10.1016/j.renene.2022.10.102.

13 B.-W. Zhang, T. Sheng, Y.-X. Wang, S. Chou, K. Davey, S.-X. Dou and S.-Z. Qiao, Long-Life Room-Temperature Sodium–Sulfur Batteries by Virtue of Transition-Metal-Nanocluster–Sulfur Interactions, *Angew. Chem., Int. Ed.*, 2019, **58**(5), 1484–1488, DOI: 10.1002/anie.201811080.

14 P. Hu, F. Xiao, Y. Wu, X. Yang, N. Li, H. Wang and J. Jia, Covalent Encapsulation of Sulfur in a Graphene/N-Doped Carbon Host for Enhanced Sodium-Sulfur Batteries, *Chem. Eng. J.*, 2022, **443**, 136257, DOI: 10.1016/j.cej.2022.136257.

15 R. K. Bhardwaj, S. Jayanthi, P. S. Adarakatti, A. K. Sood and A. J. Bhattacharyya, Probing the Extent of Polysulfide Confinement Using a CoNi2S4 Additive Inside a Sulfur Cathode of a Na/Li–Sulfur Rechargeable Battery, *ACS Appl. Mater. Interfaces*, 2020, **12**(25), 28120–28128, DOI: 10.1021/acsami.0c04507.

16 S. P. Jand, Y. Chen and P. Kaghazchi, Comparative Theoretical Study of Adsorption of Lithium Polysulfides (Li2Sx) on Pristine and Defective Graphene, *J. Power Sources*, 2016, **308**, 166–171, DOI: 10.1016/j.jpowsour.2016.01.062.

17 Q. Zhang, Y. Wang, Z. W. Seh, Z. Fu, R. Zhang and Y. Cui, Understanding the Anchoring Effect of Two-Dimensional Layered Materials for Lithium–Sulfur Batteries, *Nano Lett.*, 2015, **15**(6), 3780–3786, DOI: 10.1021/acs.nanolett.5b00367.

18 G. Babu, N. Masurkar, H. Al Salem and L. M. R. Arava, Transition Metal Dichalcogenide Atomic Layers for Lithium Polysulfides Electrocatalysis, *J. Am. Chem. Soc.*, 2017, **139**(1), 171–178, DOI: 10.1021/jacs.6b08681.

19 H. H. Haseeb, Y. Li, S. Ayub, Q. Fang, L. Yu, K. Xu and F. Ma, Defective Phosphorene as a Promising Anchoring Material for Lithium–Sulfur Batteries, *J. Phys. Chem. C*, 2020, **124**(5), 2739–2746, DOI: 10.1021/acs.jpcc.9b06023.

20 D. J. Late, C. S. Rout, D. Chakravarty and S. Ratha, Emerging Energy Applications of Two-Dimensional Layered Materials, *Can. Chem. Trans.*, 2015, **3**(2), 118–157, DOI: 10.13179/canchemtrans.2015.03.02.0174.

21 M. S. Nahian, R. Jayan, T. Kaewmaraya, T. Hussain and M. M. Islam, Elucidating Synergistic Mechanisms of Adsorption and Electrocatalysis of Polysulfides on Double-Transition Metal MXenes for Na–S Batteries, *ACS Appl. Mater. Interfaces*, 2022, **14**(8), 10298–10307, DOI: 10.1021/acsami.1c22511.

22 X. Wang, Y. Cai, S. Wu and B. Li, Sulfur Functions as the Activity Centers for High-Capacity Lithium Ion Batteries in S- and O-Bifunctionalized MXenes: A Density Functional Theory (DFT) Study, *Appl. Surf. Sci.*, 2020, **525**, 146501, DOI: 10.1016/j.apsusc.2020.146501.

23 L. Li, M. Zhao, B. Zhang, G. Shao and Y. Zhao, One-Pot Synthesis of Nitrogen-Doped Porous Carbon Derived from the *Siraitia Grosvenorii* Peel for Rechargeable Zinc–Air Batteries, *Energy Fuels*, 2023, **37**(7), 5412–5420, DOI: 10.1021/acs.energyfuels.2c04369.

24 L. Wang, T. Wang, L. Peng, Y. Wang, M. Zhang, J. Zhou, M. Chen, J. Cao, H. Fei, X. Duan, J. Zhu and X. Duan, The Promises, Challenges and Pathways to Room-Temperature Sodium-Sulfur Batteries, *Natl. Sci. Rev.*, 2022, **9**(3), nwab050, DOI: 10.1093/nsr/nwab050.

25 Y. Wang, T. Guo, E. Alhajji, Z. Tian, Z. Shi, Y.-Z. Zhang and H. N. Alshareef, MXenes for Sulfur-Based Batteries, *Adv. Energy Mater.*, 2023, **13**(4), 2202860, DOI: 10.1002/aenm.202202860.

26 Q. Zhao, Q. Zhu, Y. Liu and B. Xu, Status and Prospects of MXene-Based Lithium–Sulfur Batteries, *Adv. Funct. Mater.*, 2021, **31**(21), 2100457, DOI: 10.1002/adfm.202100457.

27 D. Rao, L. Zhang, Y. Wang, Z. Meng, X. Qian, J. Liu, X. Shen, G. Qiao and R. Lu, Mechanism on the Improved Performance of Lithium Sulfur Batteries with MXene-Based Additives, *J. Phys. Chem. C*, 2017, **121**(21), 11047–11054, DOI: 10.1021/acs.jpcc.7b00492.

28 Y.-H. Liu, L.-X. Li, A.-Y. Wen, F.-F. Cao and H. Ye, A Janus MXene/MOF Separator for the All-in-One Enhancement of Lithium-Sulfur Batteries, *Energy Storage Mater.*, 2023, **55**, 652–659, DOI: 10.1016/j.ensm.2022.12.028.

29 N. Li, Y. Zhan, H. Wu, J. Fan and J. Jia, Covalent Surface Modification of Bifunctional Two-Dimensional Metal Carbide MXenes as Sulfur Hosts for Sodium–Sulfur Batteries, *Nanoscale*, 2022, **14**(45), 17027–17035, DOI: 10.1039/D2NR03462J.

30 X. Liang, A. Garsuch and L. F. Nazar, Sulfur Cathodes Based on Conductive MXene Nanosheets for High-Performance Lithium–Sulfur Batteries, *Angew. Chem.*, 2015, **127**(13), 3979–3983, DOI: 10.1002/ange.201410174.

31 W. Bao, C. E. Shuck, W. Zhang, X. Guo, Y. Gogotsi and G. Wang, Boosting Performance of Na–S Batteries Using Sulfur-Doped Ti3C2Tx MXene Nanosheets with a Strong Affinity to Sodium Polysulfides, *ACS Nano*, 2019, **13**(10), 11500–11509, DOI: 10.1021/acsnano.9b04977.

32 X. Wang, Y. Cai, S. Wu and B. Li, Sulfur Functions as the Activity Centers for High-Capacity Lithium Ion Batteries in S- and O-Bifunctionalized MXenes: A Density Functional Theory (DFT) Study, *Appl. Surf. Sci.*, 2020, **525**, 146501, DOI: 10.1016/j.apsusc.2020.146501.

Open Access Article. Published on 01 October 2025. Downloaded on 4/1/2026 3:22:40 PM.
This article is licensed under a Creative Commons Attribution 3.0 Unported Licence.

33 W. Hong, B. C. Wyatt, S. K. Nemani and B. Anasori, Double Transition-Metal MXenes: Atomistic Design of Two-Dimensional Carbides and Nitrides, *MRS Bull.*, 2020, **45**(10), 850–861, DOI: 10.1557/mrs.2020.251.

34 S. Venkateshalu, M. Shariq, B. Kim, M. Patel, K. S. Mahabari, S.-I. K. Choi, N. Chaudhari, A. N. Grace and K. Lee, Recent Advances in MXenes: Beyond Ti-Only Systems, *J. Mater. Chem. A*, 2023, **11**(25), 13107–13132, DOI: 10.1039/D3TA01590D.

35 A. Akhoondi, M. E. Nejad, M. Yusuf, T. M. Aminabhavi, K. M. Batoo and S. Rtimi, Synthesis and Applications of Double Metal MXenes: A Review, *Synth. Sintering*, 2023, **3**(2), 107–123, DOI: 10.53063/synsint.2023.32150.

36 B. Anasori, M. R. Lukatskaya and Y. Gogotsi, 2D Metal Carbides and Nitrides (MXenes) for Energy Storage, in *MXenes*, Jenny Stanford Publishing, 2023, pp. 677–722.

37 S. Sun, C. Liao, A. M. Hafez, H. Zhu and S. W, Two-dimensional MXenes for Energy Storage, *Chem. Eng. J.*, 2017, 338, DOI: 10.1016/j.cej.2017.12.155.

38 N. Li, Z. Zeng, Y. Zhang, X. Chen, Z. Kong, Arramel, Y. Li, P. Zhang and B.-S. Nguyen, Double Transition Metal Carbides MXenes (D-MXenes) as Promising Electrocatalysts for Hydrogen Reduction Reaction: Ab Initio Calculations, *ACS Omega*, 2021, **6**(37), 23676–23682, DOI: 10.1021/acsomega.1c00870.

39 X. Song, H. Wang, S. Jin, M. Lv, Y. Zhang, X. Kong, H. Xu, T. Ma, X. Luo, H. Tan, D. Hu, C. Deng, X. Chang and J. Xu, Oligolayered Ti3C2T x MXene towards high performance lithium/sodium storage, *Nano Res.*, 2020, **13**(6), 1659–1667, DOI: 10.1007/s12274-020-2789-6.

40 V. Mehta, H. S. Saini, S. Srivastava, M. K. Kashyap and K. Tankeshwar, Ultralow Diffusion Barrier of Double Transition Metal MoWC Monolayer as Li-Ion Battery Anode, *J. Mater. Sci.*, 2022, **57**(23), 10702–10713, DOI: 10.1007/s10853-022-07237-1.

41 M. Zhou, Y. Shen, J. Liu, L. Lv, Y. Zhang, X. Meng, X. Yang, B. Zhang and Z. Zhou, Excellent Double Metal MXenes MoWC Anode: The Synergistic Effect of Molybdenum and Tungsten Transition Metal, *Vacuum*, 2023, **213**, 112152, DOI: 10.1016/j.vacuum.2023.112152.

42 R. Jayan and M. M. Islam, Functionalized MXenes as Effective Polyselenide Immobilizers for Lithium–Selenium Batteries: A Density Functional Theory (DFT) Study, *Nanoscale*, 2020, **12**(26), 14087–14095, DOI: 10.1039/D0NR02296A.

43 F. Bibi, A. Hanan, I. A. Soomro, A. Numan and M. Khalid, Double Transition Metal MXenes for Enhanced Electrochemical Applications: Challenges and Opportunities, *EcoMat*, 2024, **6**(9), e12485, DOI: 10.1002/eom2.12485.

44 R. Pritom, I. Nandi, M. S. Nahian, R. Jayan, S. Mojumder and M. M. Islam, Computational Discovery of a Novel Double Transition Metal Nitride MXene and Its Applications as an Anchoring and Catalytic Material in Li–Se Batteries, *J. Mater. Chem. A*, 2025, **13**(29), 24038–24050, DOI: 10.1039/D5TA03099D.

45 V. Wang, N. Xu, J.-C. Liu, G. Tang and W.-T. Geng, VASPKIT: A User-Friendly Interface Facilitating High-Throughput Computing and Analysis Using VASP Code, *Comput. Phys. Commun.*, 2021, **267**, 108033, DOI: 10.1016/j.cpc.2021.108033.

46 K. Momma and F. Izumi, VESTA 3 for Three-Dimensional Visualization of Crystal, Volumetric and Morphology Data, *J. Appl. Crystallogr.*, 2011, **44**(6), 1272–1276, DOI: 10.1107/S0021889811038970.

47 N. Thatsami, P. Tangpakonsab, P. Moontragoon, R. Umer, T. Hussain and T. Kaewmaraya, Two-Dimensional Titanium Carbide (Ti 3 C 2 T x) MXenes to Inhibit the Shuttle Effect in Sodium Sulfur Batteries, *Phys. Chem. Chem. Phys.*, 2022, **24**(7), 4187–4195, DOI: 10.1039/D1CP05300K.

48 C. Yao, W. Li, K. Duan, C. Zhu, J. Li, Q. Ren and G. Bai, Properties of S-Functionalized Nitrogen-Based MXene (Ti2NS2) as a Hosting Material for Lithium-Sulfur Batteries, *Nanomaterials*, 2021, **11**(10), 2478, DOI: 10.3390/nano11102478.

49 *WebElements Periodic Table "Oxygen" electronegativity.* https://winter.group.shef.ac.uk/webelements/oxygen/electronegativity.html (accessed 2025-04-15).

50 M. S. Nahian, R. Jayan and M. M. Islam, Atomic-Scale Insights into Comparative Mechanisms and Kinetics of Na–S and Li–S Batteries, *ACS Catal.*, 2022, **12**(13), 7664–7676, DOI: 10.1021/acscatal.2c01174.

51 R. Jayan and M. M. Islam, Design Principles of Bifunctional Electrocatalysts for Engineered Interfaces in Na–S Batteries, *ACS Catal.*, 2021, **11**(24), 15149–15161, DOI: 10.1021/acscatal.1c04739.

52 S. Karmakar and T. Saha-Dasgupta, First-Principles Prediction of Enhanced Thermoelectric Properties of Double Transition Metal MXenes: $Ti_{3-x}Mo_xC_2T_2$; (x=0.5,1,1.5,2,2.5, T=−OH/−O/−F), *Phys. Rev. Mater.*, 2020, **4**(12), 124007, DOI: 10.1103/PhysRevMaterials.4.124007.

53 R. Tesch and P. M. Kowalski, Hubbard U parameters for transition metals from first principles, *Phys. Rev. B*, 2022, **105**(19), 195153, DOI: 10.1103/PhysRevB.105.195153.

54 S. Berman, A. Zhussupbekova, J. E. Boschker, J. Schwarzkopf, D. D. O'Regan, I. V. Shvets and K. Zhussupbekov, Reconciling the Theoretical and Experimental Electronic Structure of NbO_2, *Phys. Rev. B: Condens. Matter Mater. Phys.*, 2023, **108**(15), 155141, DOI: 10.1103/PhysRevB.108.155141.

55 S. Deng, T. Guo, J. Heier and C. Zhang, Unraveling Polysulfide's Adsorption and Electrocatalytic Conversion on Metal Oxides for Li–S Batteries, *Adv. Sci.*, 2022, **10**(5), 2204930, DOI: 10.1002/advs.202204930.

56 W. Song, Z. Wen, X. Wang, K. Qian, T. Zhang, H. Wang, J. Ding and W. Hu, Unsaturation Degree of Fe Single Atom Site Manipulates Polysulfide Behavior in Sodium-Sulfur Batteries, *Nat. Commun.*, 2025, **16**(1), 2795, DOI: 10.1038/s41467-025-58114-9.

 This journal is © The Royal Society of Chemistry 2025

57 M. Cheng, R. Yan, Z. Yang, X. Tao, T. Ma, S. Cao, F. Ran, S. Li, W. Yang and C. Cheng, Polysulfide Catalytic Materials for Fast-Kinetic Metal–Sulfur Batteries: Principles and Active Centers, *Adv. Sci.*, 2022, **9**(2), 2102217, DOI: **10.1002/advs.202102217**.

58 R. Liu, C. Feng, P. Wu, Y. Sun, Z. Chu, J. Hu, W. Chen, L. Guo, Q. Huang and D. Wang, Improving Conversion Kinetics of Sodium Polysulfides through Electron Spillover Effect with V/Co Dual-Atomic Site Anchoring on N-Doped MXene, *Adv. Mater.*, 2025, **37**(21), 2501371, DOI: **10.1002/adma.202501371**.

Open Access Article. Published on 01 October 2025. Downloaded on 4/1/2026 3:22:40 PM.
This article is licensed under a Creative Commons Attribution 3.0 Unported Licence.